


Article

Tetraethylene Glycol Dimethyl Ether (TEGDME)-Water Hybrid Electrolytes Enable Excellent Cyclability in Aqueous Zn-Ion Batteries

Mingliang Shangguan, Kehuang Wang, Yibo Zhao and Lan Xia * 

Faculty of Maritime and Transportation, Ningbo University, Ningbo 315211, China

* Correspondence: xialan@nbu.edu.cn

Abstract: Aqueous zinc-ion batteries (AZIBs) are considered hopeful large-scale electrochemical energy storage devices because of their simple production process, high specific capacity, intrinsic safety and low cost. However, the dendritic growth of Zn and side reactions cause rapid battery performance degradation, which limits the application of AZIBs for large-scale energy storage. In this work, following the addition of tetraethylene glycol dimethyl ether (TEGDME) to 1 mol L⁻¹ (M) Zn(CF₃SO₃)₂ aqueous electrolyte as a cosolvent, the 1 M Zn(CF₃SO₃)₂/TEGDME-H₂O (1:1 by volume) hybrid electrolyte showed enhanced battery performance resulting from the expanding electrochemical window, inhibiting the growth of zinc dendrites and the parasitic reactions on the negative Zn electrode. The experimental results show that this hybrid electrolyte enabled a high coulombic efficiency (CE) of >99% for 200 cycles in the Zn | | Cu battery and a steady discharge/charge property for 1000 h with a low overpotential of 100 mV at 1 mA cm⁻² (the capacity: 1.13 mAh) in the Zn | | Zn battery. Remarkably, Zn | | V₂O₅ batteries with the hybrid electrolyte also performed much better in terms of cycling stability than a device with a 1 M Zn(CF₃SO₃)₂ aqueous electrolyte. Zn | | V₂O₅ batteries delivered a high specific capacity of 200 mAh g⁻¹ with an average CE of >99.9% after 1500 cycles at 0.5 A g⁻¹. This study provides a promising strategy for the development of high-performance electrolyte solutions for practical rechargeable AZIBs.



Citation: Shangguan, M.; Wang, K.; Zhao, Y.; Xia, L. Tetraethylene Glycol Dimethyl Ether (TEGDME)-Water Hybrid Electrolytes Enable Excellent Cyclability in Aqueous Zn-Ion Batteries. *Batteries* **2023**, *9*, 462. <https://doi.org/10.3390/batteries9090462>

Academic Editor: John R Owen

Received: 2 August 2023

Revised: 1 September 2023

Accepted: 7 September 2023

Published: 11 September 2023



Copyright: © 2023 by the authors. Licensee MDPI, Basel, Switzerland. This article is an open access article distributed under the terms and conditions of the Creative Commons Attribution (CC BY) license (<https://creativecommons.org/licenses/by/4.0/>).

Keywords: aqueous zinc-ion battery; electrolyte; cosolvent; tetraethylene glycol dimethyl ether; vanadium pentoxide

1. Introduction

In recent years, with the vigorous development of portable electronic devices, electric vehicles and clean energy [1], lithium-ion batteries have occupied most of the market because of their high energy density and power density. However, their limited resources, high cost and low safety limit their widespread application [2]. In contrast, aqueous Zn-ion batteries (AZIBs) have the advantages of high theoretical capacity (820 mAh g⁻¹) and low redox potential (−0.76 V vs. standard hydrogen electrode) [3]. AZIBs are also considered to be promising as energy storage devices. Most importantly, Zn reserves are abundant, and Zn is available for a low price and is highly compatible with water in air [4]. A simple manufacturing and assembly process is a key factor in the potential commercialization of aqueous zinc-ion batteries [5]. However, the large amount of water in the aqueous electrolyte leads to parasitic reactions and rapid growth of Zn dendrites [6], resulting in battery failure. During the deposition of zinc, the strong interaction between the solvated structure of Zn²⁺ and the surrounding H₂O molecules accelerates the occurrence of parasitic reactions [7]. In the plating/stripping process of zinc metal, water decomposes into H₂, and the local pH environment caused by the hydrogen evolution reaction further increases the generation of byproducts [8], promotes corrosion, hinders ion transport [9] and reduces the utilization rate of Zn [10]. These problems may lead to penetration of the separator, serious corrosion and even battery failure, which seriously limit the

large-scale application of aqueous zinc-ion batteries [11]. Several effective strategies have been proposed to solve these challenging problems, such as changing the structure of the electrode material, modifying the separator and optimizing the electrolyte formulation [12]. Overall, optimizing the electrolyte formulation is a simple and effective way to build a functional interface layer on the surface of Zn metal [13–15].

The optimization of electrolytes is divided into solute (including zinc salts, additives and high-concentration salts) and solvent aspects [16]. In a water-based zinc-ion electrolyte, in addition to the hydrogen bond between water molecules and the force between Zn^{2+} – H_2O , there are also forces between anions and H_2O . Since ions are charged, the force between anions and water is stronger than the hydrogen bond between water molecules, which can destroy the structure of the hydrogen bond network between water molecules and participate in the solvation process of Zn^{2+} [17]. By comparing electrochemical impedance spectroscopic (EIS) images of zinc-ion electrolytes with the same concentration of ZnSO_4 , ZnCl_2 , $\text{Zn}(\text{NO}_3)_2$, $\text{Zn}(\text{CH}_3\text{COO})_2$ and $\text{Zn}(\text{CF}_3\text{SO}_3)_2$, Wang et al. [18] found that the order of diffusion impedance of Zn^{2+} is $\text{ZnCl}_2 < \text{Zn}(\text{CF}_3\text{SO}_3)_2 < \text{ZnSO}_4 < \text{Zn}(\text{CH}_3\text{COO})_2 < \text{Zn}(\text{NO}_3)_2$, indicating that in ZnCl_2 electrolytes, Zn^{2+} has the fastest migration rate at the electrode material/electrolyte interface. However, the stability of the electrochemical window for ZnCl_2 electrolytes is narrow, leading to the decomposition of electrolytes at higher potentials. In contrast, the CF_3SO_3^- anion in $\text{Zn}(\text{CF}_3\text{SO}_3)_2$ salt has a large volume and can reduce the amount of free water around Zn^{2+} , thereby further reducing the solvation effect. Moreover, Zn^{2+} exhibits higher level of reversibility and faster reaction kinetics in $\text{Zn}(\text{CF}_3\text{SO}_3)_2$ electrolytes. The positive electrode material exhibits good electrochemical performance in $\text{Zn}(\text{CF}_3\text{SO}_3)_2$ [19]. Therefore, in this article, we choose $\text{Zn}(\text{CF}_3\text{SO}_3)_2$ salts as the solute of the electrolyte. Solvents are another important component of electrolyte components [20], and solvent regulation mainly involves mixing organic solvents that can blend with water in different proportions. Their influence on the electrochemical performance of aqueous ZIBs mainly depends on the relative content and the solvation effect between them and Zn^{2+} . Organic solvents such as acetonitrile (ACN) [21], dimethyl sulfoxide (DMSO) [22], ethyl ether [23], alcohols (methanol, ethanol, ethylene glycol, glycerol, etc.) [24], acrylamide (AM) [25], triethyl phosphate (TEP) [26], etc., can decrease the solvation structure of Zn^{2+} and participate in recombination, reducing the number of water molecules in the solvent sheath structure. Li et al. [27] used $\text{Li}_3\text{V}_2(\text{PO}_4)_3$ as the positive electrode material and compared the electrochemical behavior and performance in $1 \text{ mol kg}^{-1} \text{ Zn}(\text{ClO}_4)_2$ aqueous solution and $1 \text{ mol kg}^{-1} \text{ Zn}(\text{ClO}_4)_2$ hybrid electrolyte of acetonitrile and water ($\text{ACN-H}_2\text{O}$). The capacity of $\text{Li}_3\text{V}_2(\text{PO}_4)_3$ electrode material rapidly decreases in aqueous electrolyte, possibly due to the dissolution of the positive electrode material in the aqueous electrolyte [28]. In $\text{ACN-3\% H}_2\text{O}$ hybrid electrolytes, the cycling stability significantly increases, and after 200 cycles, there is still a remaining capacity of 87 mAh g^{-1} . When the water content further increases ($\text{ACN-11\% H}_2\text{O}$), the initial capacity of the battery can reach 125 mAh g^{-1} . After 200 cycles, the capacity is still 121 mAh g^{-1} .

In previous reports of solvent regulation, most organic solvents had a low molecular weight, as well as low melting and boiling points. If the temperature is too high, some negative chemical reactions occur inside the battery, affecting the battery life and even safety performance [29]. Therefore, selecting organic cosolvents with high molecular weights is beneficial in terms of improving the safety of batteries. In previous literature, tetraethylene glycol dimethyl ether (TEGDME; M_n : 222.28 g/mol ; boiling point: $275 \text{ }^\circ\text{C}$) was reported as a cosolvent in magnesium-ion batteries, achieving excellent battery performance [30]. In this work, we selected a long chain ether—tetraethylene glycol dimethyl ether (TEGDME) with a high boiling point of $275.3 \text{ }^\circ\text{C}$ and used as an organic cosolvent for aqueous zinc-ion batteries [31]. Electrolyte optimization focuses on organic solvents that are easy to operate and cost-effective. A $1 \text{ M Zn}(\text{CF}_3\text{SO}_3)_2/\text{TEGDME-H}_2\text{O}$ hybrid electrolyte was designed, and we report that introducing TEGDME into water can effectively reduce water content. The interaction between TEGDME and H_2O was stronger than that between H_2O and

H₂O, which can decrease the activity of water and inhibit the growth of zinc dendrites and the occurrence of side reactions. This study shows that 1 M Zn(CF₃SO₃)₂/TEGDME-H₂O hybrid electrolytes can enhance battery properties by expanding the electrochemical stability window. TEGDME also preferentially solvates with Zn²⁺, changes the solvation structure of Zn²⁺, inhibits parasitic reactions and improves the storage performance of zinc ions. The results of this study indicate the feasibility of using aqueous zinc-ion batteries as large-scale energy storage devices. Zn||V₂O₅ batteries with the reported hybrid electrolyte also perform much better in terms of cycling stability than a device with a 1 M Zn(CF₃SO₃)₂ aqueous electrolyte.

2. Materials and Methods

V₂O₅ synthesis: To obtain V₂O₅ powders with high purity and stable properties, V₂O₅ powder was prepared by hydrothermal method [32]. Commercial V₂O₅ (20 mmol, Shanghai Yongchuan Biotechnology Co., Ltd., Shanghai, China; AR, 99.0%) was dissolved in a mixed solution containing 60 mL deionized water and 40 g ethylene glycol (McClean, AR, 98%) and vigorously stirred to obtain a homogeneous solution. The mixture was transferred to a 200 mL autoclave and heated at 200 °C for 24 h. After cooling to room temperature, the collected products were centrifuged at 80 °C, washed and dried for 12 h. The V₂O₅ powder was obtained by annealing the products at 330 °C for 30 min at a heating rate of 2 °C min⁻¹ [33].

Electrolyte preparation: An amount of 3.64 g Zn(CF₃SO₃)₂ (purity: 98%) was dissolved in 10 mL tetraethylene glycol dimethyl ether (TEGDME, purity: 99%) and a deionized water solvent mixture with volume ratios of TEGDME to deionized water were 1:0, 1:1, 1:2, 1:3, 2:1, 3:1 and 0:1. Both Zn(CF₃SO₃)₂ and TEGDME were used directly without any treatment. When a volume ratio of TEGDME to H₂O of 1:0 was labeled as TEGDME, a volume ratio of TEGDME to H₂O of 1:1 was labeled as 1:1, etc. Thus, the molar concentration of Zn(CF₃SO₃)₂ salt in all electrolytes was fixed at 1 mol L⁻¹.

Material characterization: A field emission scanning electron microscope (SEM, S4800, Hitachi, Tokyo, Japan) was used to obtain the surface morphology of V₂O₅ powders and the electrode. The solvation structure of electrolytes was investigated using a Fourier transform infrared spectrometer (FTIR, Nicolet6700, Thermo Fisher Scientific, Carlsbad, CA, US) and Raman spectrometer (inVia Reflex, Renishaw, Wotton-under-Edge, UK). An X-ray diffractometer (XRD, D8 DISCOVER, Bruker, Mannheim, Germany) was used to obtain X-ray diffraction (XRD) patterns of the surface composition on the Cu foil.

Electrochemical measurements: The V₂O₅ powder was mixed with conductive carbon (Super P) and polyvinylidene fluoride (PVDF) at a mass ratio of 7:2:1 to prepare the V₂O₅ positive electrode. After 8 h of mixing with a magnetic stirrer, the slurry was painted on titanium foil with a thickness of 0.01 mm and dried at 90 °C for 12 h. The dried material was then cut into a circular sheet with a diameter of 12 mm and a thickness of 0.1 mm. The amount of active substance in the V₂O₅ positive electrode was about 2 mg. Zn metal was also cut into circular slices with a diameter of 12 mm and a thickness of 0.1 mm. The positive electrode, the fiberglass diaphragm and the negative electrode were assembled using CR2032-type coin cells in an air atmosphere. The electrolyte used in the assembly process was approximately 110 µL. Using the CHI660e electrochemical workstation, stainless steel as positive electrode and zinc as negative electrode, the linear sweep voltammetry (LSV) curve at the range of 0 to 2.8 V was determined to test the electrochemical window of the electrolyte. The scanning rate was 1 mV s⁻¹. The conductivity of the electrolyte was measured by a conductivity meter (DDSJ-308F). Electrochemical impedance spectroscopy (EIS) was carried out using an electrochemical workstation. To test the Zn²⁺ deposition potential of the electrolyte, the cyclic voltammetry (CV) curve was measured by an electrochemical workstation. A Land CT2001A battery testing system (Wuhan Land Electronic Co., Ltd., Wuhan, China) was used to test the galvanostatic charge/discharge (GCD) and rate performance.

3. Results and Discussion

3.1. Properties of 1 M $Zn(CF_3SO_3)_2$ TEGDME/ H_2O Hybrid Electrolyte

Using V_2O_5 powder as a positive electrode and zinc foil as a negative electrode, we fabricated a $Zn || V_2O_5$ battery to test the cycling stability, specific capacity and coulombic efficiency (CE) of a series of TEGDME/ H_2O hybrid electrolytes at room temperature ($25^\circ C$). Figure 1a shows the long-term cycling properties of the $Zn || V_2O_5$ battery at $0.5 A g^{-1}$. For the 1:3 hybrid electrolyte, the capacity increases dramatically to $350 mA h g^{-1}$ during the first 10 cycles, then decays to $220 mA h g^{-1}$ after 200 cycles. However, the 3:1 hybrid electrolyte maintains a low capacity of $140 mA h g^{-1}$ after 200 cycles. It is encouraging that 1:1 and 1:2 hybrid electrolytes exhibit good cycling stability and deliver a high reversible capacity of 300 and $240 mA h g^{-1}$, with corresponding capacity retentions as high as 91.7% and 89.5% and an average CE of $>99.9\%$ and 98.8% after 200 cycles, respectively. However, the specific capacity of batteries using both H_2O alone and a TEGDME electrolyte is only 77.1 and $75.5 mA h g^{-1}$, with only 26% and 61% capacity retention maintained after 200 cycles, respectively. The enhanced cycling properties of batteries containing TEGDME/ H_2O hybrid electrolytes suggests that the addition of TEGDME cosolvent changes the solvation effect of the aqueous ZIBs electrolyte.

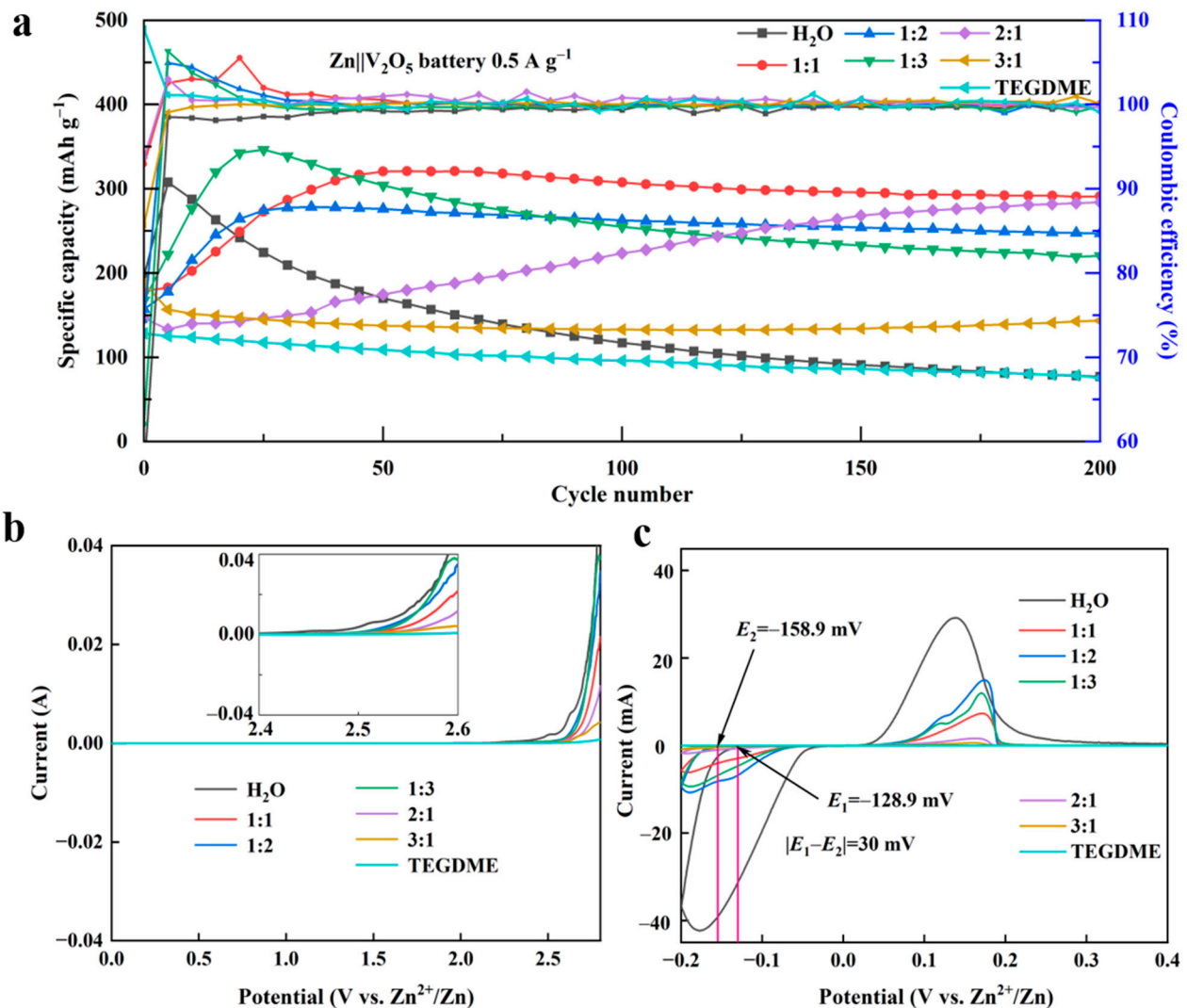


Figure 1. (a) Long-term cycling performance of a $Zn || V_2O_5$ battery assembled with different hybrid electrolytes at $0.5 A g^{-1}$, (b) LSV profiles of $Zn ||$ stainless-steel (SS) cells with different hybrid electrolytes at $0.1 mV s^{-1}$ and (c) CV profiles of $Zn ||$ SS cells at $1 mV s^{-1}$.

The LSV and CV curves of Zn || stainless-steel (SS) batteries were used to further investigate the electrochemical stability of TEGDME/H₂O hybrid electrolytes. The LSV curves show that as the content of water decreases and the content of TEGDME increases, the oxidation potential of the hybrid electrolyte increases. Notably, the oxidative current of a 1:1 hybrid electrolyte is observed above 2.5 V vs. Zn²⁺/Zn, suggesting that the 1:1 hybrid electrolyte has high oxidative stability compared to 1 M Zn(CF₃SO₃)₂ in pure H₂O. The CV curves of batteries assembled with different electrolytes are displayed in Figure 1c. As the water content increases, the oxidation potential of the hybrid electrolyte increases, i.e., the redox reaction of H₂O electrolytes. Therefore, the peak of batteries with water electrolytes is higher than batteries with hybrid electrolytes. The nucleation overpotential of H₂O electrolytes is 128.9 mV, while the nucleation overpotential of 1:1 hybrid electrolytes increases to 158.9 mV. A high nucleation overpotential means a strong driving force for nucleation, enabling production of good crystalline deposits [34], while a low nucleation overpotential likely leads to Zn dendrites due to the tip effect [35]. Therefore, a high nucleation overpotential can optimize the morphology of Zn deposition in a 1:1 hybrid electrolyte. In addition, the peak intensity of the CV curve indicates the reaction kinetics of electrolytes. The radius of the [Zn(H₂O)_m(TEGDME)_n]²⁺ complex is larger than that of [Zn(H₂O)₆]²⁺, resulting in slower diffusion of hybrid electrolytes, lower peak intensity and slower reaction kinetics in hybrid electrolytes [36].

As shown in Figure 2a, the FTIR spectra of H₂O electrolytes have strong O–H stretching vibrations between 3000 and 3500 cm^{−1} and strong H₂O bending vibrations between 1600 and 1700 cm^{−1}, which come from the free water molecules. In the 1:1 hybrid electrolyte, these two characteristic bands show a slight blue shift, indicating that TEGDME cosolvents disturb the hydrogen bond interaction between H₂O molecules [37]. The blue shift of the H–O bond suggests that the H–O covalent bond strength of H₂O in TEGDME hybrid electrolytes increases, improving the stability of the electrolyte. Raman spectra are also shown in Figure 2b; the typical –CH₂ and –CH₃ vibrational bands of the TEGDME hybrid electrolyte at 2800–3000 cm^{−1} gradually increase with the increase in the TEGDME content, which is attributed to the different hydrogen bond environments. This can be attributed to the coordination between H₂O and TEGDME [38], which is beneficial in reducing the side reactions between free water and the electrode, thereby inhibiting potential damage to the electrode material [30]. After adding TEGDME into hybrid electrolytes, the ionic conductivity of the electrolyte (i.e., the conductivity of Zn²⁺) decreases with the increase in the TEGDME content (Figure 2c) because of the slower reaction kinetics, resulting in decreased mass transfer, inhibiting the rapid growth of Zn dendrites, facilitating the uniform deposition of Zn on the surface of the electrode and improving the electrochemical performance of TEGDME hybrid electrolytes.

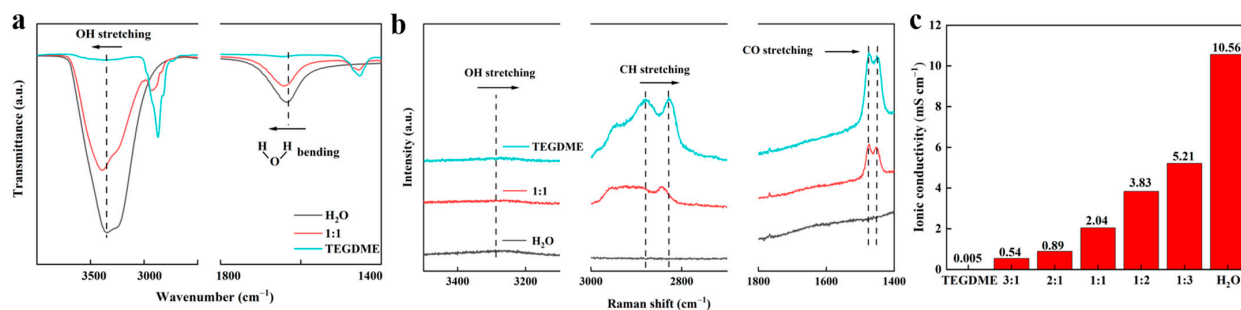


Figure 2. (a) FTIR spectra, (b) Raman spectra and (c) ionic conductivity of a series of hybrid electrolytes at room temperature.

3.2. Electrochemical Properties of Various Hybrid Electrolytes

The Coulombic efficiency (CE) of the Zn || Cu half-cells was measured under the condition of a current density of 1 mA cm^{−2}. The charge cutoff voltage was 1 V, and the discharge time was 1 h at room temperature (25 °C). As shown in Figure 3a, for the

H₂O electrolyte, the average CE of a Zn || Cu battery is 97% in the first 55 cycles, while the CE quickly fluctuates after 55 cycles. In contrast, the coulombic efficiency (CE) of a Zn || Cu battery with a 1:1 hybrid electrolyte remains stable >99% for 200 cycles. The improved performance may be caused by the significant suppression of Zn dendrites and side reactions in the 1:1 hybrid electrolyte. Figure 3b displays the specific voltage curves in the H₂O electrolyte; the voltage is very unstable during the cycle, which results in battery failure [39]. However, the 1:1 hybrid electrolyte shows significantly improved CE and stable curves (Figure 3c), with an average coulombic efficiency >99% from the 2nd to 200th cycle. In addition, the surface composition formed on the Cu surface was analyzed using XRD. The XRD pattern of the surface composition on the Cu foil surface cycled in the H₂O electrolyte shows a relatively weak Zn_x(CF₃SO₃)_y(OH)_{2x-y}·nH₂O peak [40], indicating that TEGDME can inhibit the production of byproducts (Figure 3d). In order to further investigate the effect of TEGDME on the Cu electrode, the surface morphology of a Cu electrode after Zn deposition for 20 h was characterized by SEM, as shown in Figure 3e,f. After Zn deposition for 20 h, the surface of the Cu electrode in the 1:1 hybrid electrolyte was smooth and uniform, with no obvious Zn aggregates, while the surface of the Cu electrode assembled with the H₂O electrolyte was loose and uneven, with many large aggregates. The results show that TEGDME cosolvent can regulate the formation of Zn dendrites and enhance the stability of batteries.

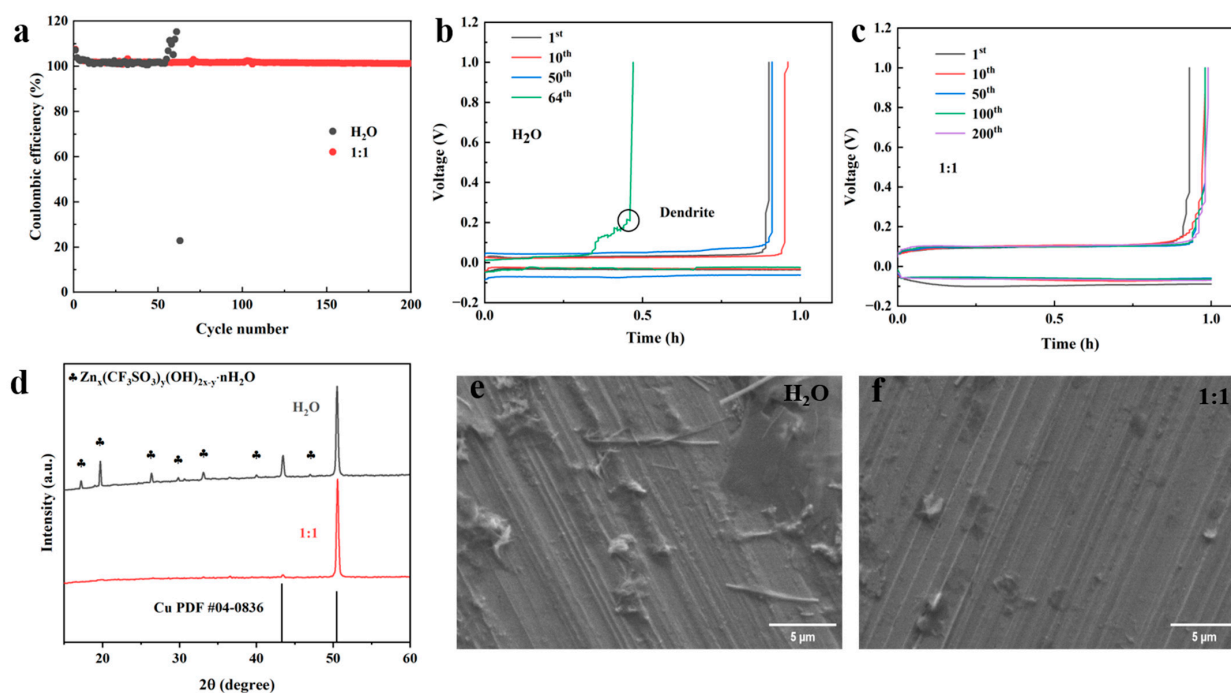


Figure 3. Characterizations of Zn || Cu batteries in H₂O and 1:1 hybrid electrolytes: (a) Coulombic efficiency of Zn plating/stripping, (b,c) voltage profiles of Zn plating/stripping processes at different cycles, (d) XRD profiles of the surface composition of the Cu electrode after 20 h Zn plating/stripping in H₂O (gray) and 1:1 hybrid (red) electrolyte, (e,f) SEM images of the deposited Zn on the Cu electrode after 20 h.

The long-term cycling stability of the symmetric Zn || Zn batteries in H₂O and the 1:1 hybrid electrolyte is shown in Figure 4a,b. In Figure 4a,b. For these two electrolytes, a sudden jump was observed at the very beginning of the voltage profile because of the battery's initially poor wettability. As shown in Figure 4a, after cycling for 374 h at a current density of 0.2 mA cm⁻² and an area capacity of 0.2 mAh cm⁻², the battery polarization voltage in the H₂O electrolyte increased, and the battery was probably short-circuited. In contrast, the battery with a 1:1 hybrid electrolyte exhibited a stable polarization voltage without any potential fluctuations or short circuits, even at 500 h. This suggests that the

1:1 hybrid electrolyte has a stable Zn stripping/plating process. The overpotential of the TEGDME-containing battery is higher than that of the H₂O electrolyte, which is related to the decreased ionic conductivity. The polarization of Zn || Zn batteries with hybrid electrolytes is much higher than that of batteries with H₂O as electrolytes because the ionic conductivity of the hybrid electrolyte is lower than that of the H₂O electrolyte. The higher overpotential and the smoother zinc deposition of Zn || Zn batteries in the 1:1 hybrid electrolyte may be beneficial in terms of improving the stability of the battery [41]. As a result, batteries containing TEGDME have smoother zinc deposition and more stable long-term cycle performance. When the current density is increased to 1 mA cm⁻², the polarization voltages of batteries in the 1:1 hybrid electrolyte are still below 200 mV. However, the Zn || Zn battery with an H₂O electrolyte suffered from short circuits after 316 h (Figure 4b). This indicates that the 1:1 hybrid electrolyte is a promising substitute for aqueous ZIBs at a wide current density.

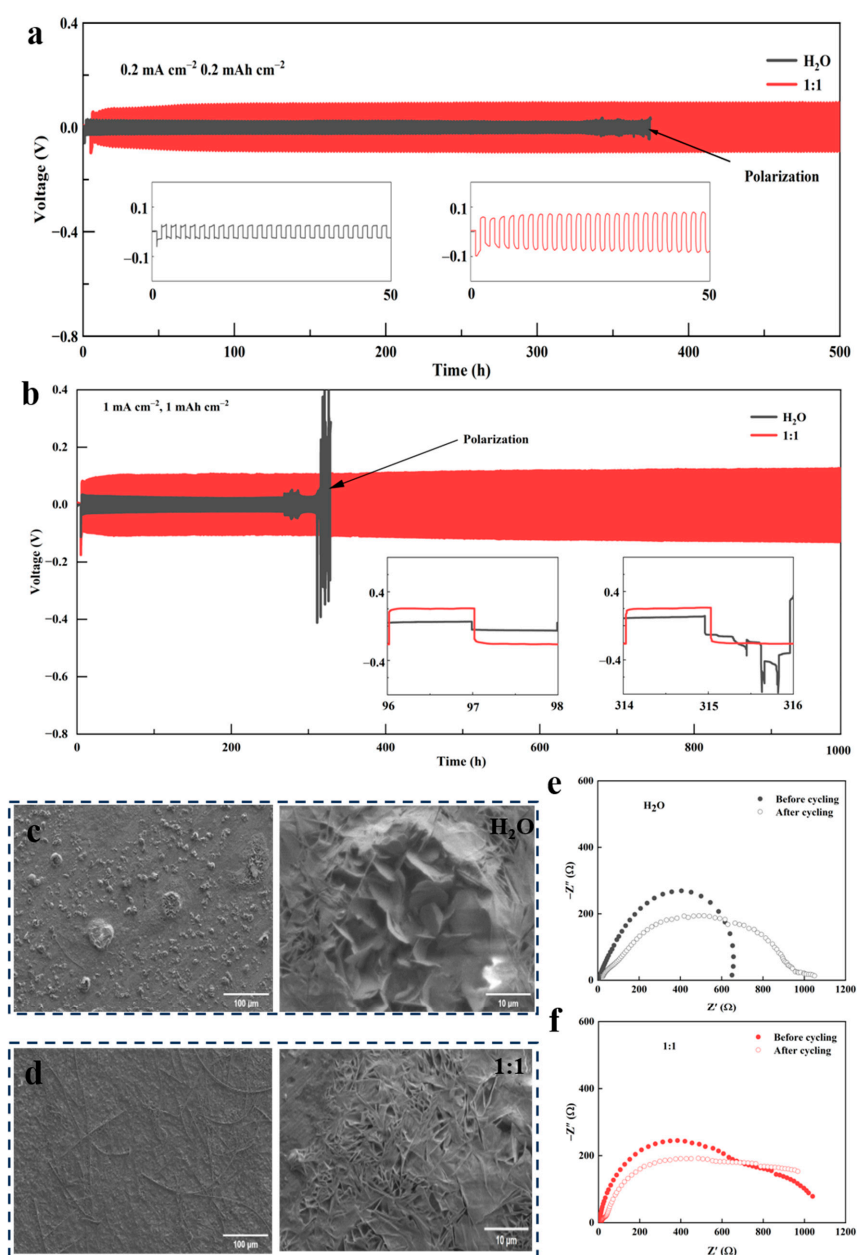


Figure 4. Characterizations of Zn || Zn symmetrical batteries in H₂O and 1:1 hybrid electrolyte. (a,b) Galvanostatic Zn plating/stripping profiles, (c,d) SEM images of a Zn electrode after 40 h and (e,f) EIS curves of Zn || Zn symmetric cells before and after 200 h.

The surface morphology and electrochemical impedance of the cycled Zn negative electrode were characterized by SEM and electrochemical impedance spectroscopy (EIS). The SEM morphology of the Zn electrode after deposition for 40 h is shown in Figure 4c,d. The surface of the Zn electrode in the H₂O electrolyte shows many flakes, which may be due to continuous side reactions. In contrast, for the 1:1 hybrid electrolyte, the electrode surface is uniform, and there are no large particle products. The EIS images of Zn || Zn batteries in H₂O and 1:1 hybrid electrolyte before and after cycling are collected in Figure 4e,f. Each of these EIS spectra has only one semicircle, which indicates a charge transfer at the electrode/electrolyte interface [42]. After cycling for 40 h, the impedance values of the 1:1 electrolyte show a slight decrease, while the impedance values in the H₂O electrolyte significantly increase. The decreased impedance values in the 1:1 hybrid electrolyte is the result of the inhibiting effect of TEGDME on byproducts during the cycling process. As a result of the decrease in water activity and the increase in the electrochemical stability window, the decomposition of water molecules is decreased, leading to a reduction in the production of OH⁻ and ultimately inhibiting the formation of the Zn_x(CF₃SO₃)_y(OH)_{2x-y}·nH₂O byproducts. These results suggest that using TEGDME as a cosolvent can suppress the formation of byproducts and dendrites, thereby providing continuous protection of the Zn negative electrode.

3.3. Characterization of Zn || V₂O₅ Batteries

To investigate the feasibility of 1:1 hybrid electrolytes for practical applications, we use them in Zn || V₂O₅ coin cells assembled in air. The cyclic voltammetry (CV) curve of the Zn || V₂O₅ cell in 1:1 hybrid electrolyte was tested at a scan rate of 0.2 mV s⁻¹ (Figure 5a). Two pairs of redox peaks appeared in the first two cycles, which means TEGDME has no influence on the redox reaction. However, the gap between the redox peak positions increases, which means that the reaction kinetics of the TEGDME hybrid electrolyte are relatively slow. This result is related to its low ionic conductivity. Figure 5b,c show the charge and discharge curves of Zn || V₂O₅ cells with H₂O and a 1:1 hybrid electrolyte at 0.5 A g⁻¹. The low specific capacity of the cell in the hybrid electrolyte during the 1st cycle and 10th cycles may be due to the activation of the battery. With the increase in the cycle number, the battery with a 1:1 hybrid electrolyte delivers a high capacity of ~250 mAh g⁻¹ and excellent cycling stability. Figure 5d shows the cyclic stability and CE curve of the Zn || V₂O₅ battery with a 1:1 hybrid electrolyte at a current density of 0.5 A g⁻¹ at room temperature. During the first 50 cycles, due to the activation process of the battery, the specific capacity of the cell in the 1:1 hybrid electrolyte rapidly increases. For the subsequent 200 cycles, the battery with this hybrid electrolyte presents a high capacity of 300 mAh g⁻¹, and the reversible capacity is maintained at 200 mAh g⁻¹, with an average coulombic efficiency of around 100%, even after 1500 cycles. However, the specific capacity of the cell in the H₂O electrolyte decreases quickly, and the battery short-circuits after 500 cycles. Although the pure TEGDME electrolyte has good cycling stability, its specific capacity is <50 mAh g⁻¹, indicating slow ion diffusion and slow kinetics. This means that cells assembled with 1:1 hydride electrolytes have excellent cycling performance due to the inhibition of water activity and dendrite growth, indicating that high capacity and long-term cycling stability of the battery are achieved with a TEGDME/H₂O electrolyte.

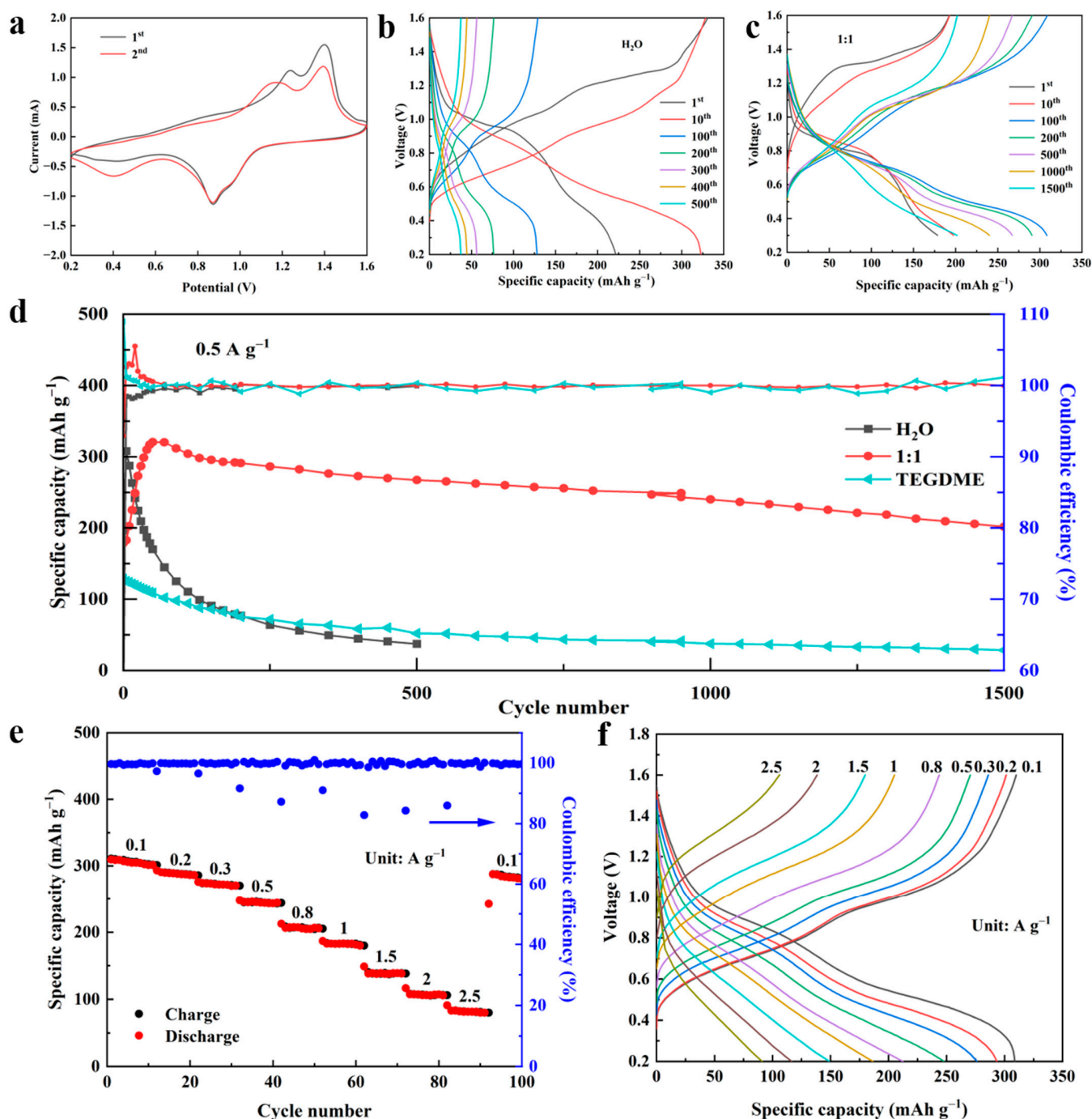


Figure 5. Cycling stability and performance of the Zn || V₂O₅ battery: (a) CV curve of Zn || V₂O₅ battery with a 1:1 hybrid electrolyte at a scan rate of 0.2 mV s⁻¹, (b,c) galvanostatic charge/discharge (GCD) curves of Zn || V₂O₅ batteries with H₂O and 1:1 hybrid electrolytes at a current density of 0.5 A g⁻¹, (d) long-term cycling performance of a Zn || V₂O₅ battery at 0.5 A g⁻¹, (e) rate performance of the cells in a 1:1 hybrid electrolyte and (f) GCD curves of the cells in a 1:1 hybrid electrolyte at different current densities.

In order to verify the reversibility and stability of the cell in a 1:1 hybrid electrolyte at different current densities, rate performance tests were performed on V₂O₅ cells (Figure 5e,f). Figure 5f shows the charge and discharge curves under different current densities. The Zn || V₂O₅ battery with the 1:1 electrolyte exhibits reversible capacities of 315, 293, 248, 213, 189, 150, 117 and 92 mAh g⁻¹ at current densities of 0.1, 0.2, 0.5, 0.8, 1, 1.5, 2.0

and 2.5 A g^{-1} , respectively. When the current density decreases back to 0.1 mA g^{-1} , the capacities immediately recover back to $\sim 310 \text{ mAh g}^{-1}$. The corresponding charge–discharge curves are displayed in Figure 5f. There are two obvious discharge/charge profiles, which means two reaction processes related to Zn^{2+} intercalation/deintercalation, in accordance with some previous reports [43,44]. Thus, this result shows that batteries using a 1:1 hybrid electrolyte have excellent rate performance, and TEGDME/ H_2O electrolytes can not only inhibit the growth of byproducts but also maintain good cycling stability of the battery.

4. Conclusions

In summary, we added TEGDME cosolvent to aqueous $1 \text{ M Zn}(\text{CF}_3\text{SO}_3)_2/\text{H}_2\text{O}$ electrolyte. The prepared 1:1 hybrid electrolyte ($1 \text{ M Zn}(\text{CF}_3\text{SO}_3)_2/\text{TEGDME}+\text{H}_2\text{O}$ (1:1 by volume)) can regulate the solvation effect of aqueous Zn^{2+} , leading to reduced water activity, inhibited growth of Zn dendrites and side reactions and improved battery performance. Remarkably, for the 1:1 hybrid electrolyte, the high cycling stability of $\text{Zn}|\text{Zn}$ symmetric batteries over 1000 h and the average CE $>99\%$ in $\text{Zn}|\text{Cu}$ asymmetric batteries were achieved. Meanwhile, $\text{Zn}|\text{V}_2\text{O}_5$ batteries with this hybrid electrolyte also performed much better than a device with a $1 \text{ M Zn}(\text{CF}_3\text{SO}_3)_2$ aqueous electrolyte in terms of cycling stability. $\text{Zn}|\text{V}_2\text{O}_5$ batteries with this hybrid electrolyte deliver a stable specific capacity of 200 mA h g^{-1} and an average coulombic efficiency of around 100% at 0.5 A g^{-1} after 1500 cycles, which is much better than batteries with a H_2O electrolyte. This study provides a promising strategy for the development of high-performance electrolyte solutions for practical rechargeable AZIBs.

Author Contributions: Conceptualization, L.X.; methodology, M.S.; formal analysis, K.W.; investigation, M.S.; data curation, Y.Z.; writing—original draft preparation, M.S.; writing—review and editing, L.X.; project administration, L.X.; supervision, L.X.; funding acquisition, L.X. All authors have read and agreed to the published version of the manuscript.

Funding: The authors are thankful for support from the National Natural Science Foundation of China (no. 22075155) and the Ningbo Science & Technology Innovation 2025 Major Project (no. 2021Z121).

Data Availability Statement: This paper contains no supporting data.

Conflicts of Interest: The authors declare no conflict of interest.

References

1. Jin, H.; Li, J.; Yuan, Y.; Wang, J.; Lu, J.; Wang, S. Recent Progress in Biomass-Derived Electrode Materials for High Volumetric Performance Supercapacitors. *Adv. Energy Mater.* **2018**, *8*, 1801007. [[CrossRef](#)]
2. Li, M.; Lu, J.; Chen, Z.; Amine, K. 30 Years of Lithium-Ion Batteries. *Adv. Mater.* **2018**, *30*, 1800561. [[CrossRef](#)]
3. Wan, F.; Zhang, L.; Dai, X.; Wang, X.; Niu, Z.; Chen, J. Aqueous rechargeable zinc/sodium vanadate batteries with enhanced performance from simultaneous insertion of dual carriers. *Nat. Commun.* **2018**, *9*, 1656. [[CrossRef](#)]
4. Li, T.C.; Fang, D.; Zhang, J.; Pam, M.E.; Leong, Z.Y.; Yu, J.; Li, X.L.; Yan, D.; Yang, H.Y. Recent progress in aqueous zinc-ion batteries: A deep insight into zinc metal anodes. *J. Mater. Chem. A* **2021**, *9*, 6013. [[CrossRef](#)]
5. Yao, M.; Yuan, Z.; Li, S.; He, T.; Wang, R.; Yuan, M.; Niu, Z. Scalable Assembly of Flexible Ultrathin All-in-One Zinc-Ion Batteries with Highly Stretchable, Editable, and Customizable Functions. *Adv. Mater.* **2021**, *33*, 2008140. [[CrossRef](#)]
6. He, M.; Shu, C.; Hu, A.; Zheng, R.; Li, M.; Ran, Z.; Long, J. Suppressing dendrite growth and side reactions on Zn metal anode via guiding interfacial anion/cation/ H_2O distribution by artificial multi-functional interface layer. *Energy Storage Mater.* **2022**, *44*, 452–460. [[CrossRef](#)]
7. Yan, H.; Li, S.; Xu, H.; Chen, H.; Yang, S.; Li, B. Triggering Zn^{2+} Unsaturated Hydration Structure via Hydrated Salt Electrolyte for High Voltage and Cycling Stable Rechargeable Aqueous Zn Battery. *Adv. Energy Mater.* **2022**, *12*, 2201599. [[CrossRef](#)]
8. Li, X.; Wang, X.; Ma, L.; Huang, W. Solvation Structures in Aqueous Metal-Ion Batteries. *Adv. Energy Mater.* **2022**, *12*, 2202068. [[CrossRef](#)]
9. Dong, C.; Xu, F.; Chen, L.; Chen, Z.; Cao, Y. Design Strategies for High-Voltage Aqueous Batteries. *Small Struct.* **2021**, *2*, 2100001. [[CrossRef](#)]
10. Li, B.; Xue, J.; Han, C.; Liu, N.; Ma, K.; Zhang, R.; Wu, X.; Dai, L.; Wang, L.; He, Z. A hafnium oxide-coated dendrite-free zinc anode for rechargeable aqueous zinc-ion batteries. *J. Colloid Interf. Sci.* **2021**, *599*, 467–475. [[CrossRef](#)]

11. Zhao, D.; Chen, S.; Lai, Y.; Ding, M.; Cao, Y.; Chen, Z. A stable “rocking-chair” zinc-ion battery boosted by low-strain $\text{Zn}_3\text{V}_4(\text{PO}_4)_6$ cathode. *Nano Energy* **2022**, *100*, 107520. [[CrossRef](#)]
12. Du, W.; Ang, E.H.; Yang, Y.; Zhang, Y.; Ye, M.; Li, C.C. Challenges in the material and structural design of zinc anode towards high-performance aqueous zinc-ion batteries. *Energy Environ. Sci.* **2020**, *13*, 3330. [[CrossRef](#)]
13. Zhang, Q.; Luan, J.; Tang, Y.; Ji, X.; Wang, H. Interfacial Design of Dendrite-Free Zinc Anodes for Aqueous Zinc-Ion Batteries. *Angew. Chem. Int. Ed.* **2020**, *59*, 13180–13191. [[CrossRef](#)]
14. Meng, C.; He, W.; Tan, H.; Wu, X.; Liu, H.; Wang, J. A eutectic electrolyte for an ultralong-lived Zn// V_2O_5 cell: An in situ generated gradient solid electrolyte interphase. *Energy Environ. Sci.* **2023**, *16*, 3587–3599. [[CrossRef](#)]
15. Hu, P.; Yan, M.; Zhu, T.; Wang, X.; Wei, X.; Li, J.; Zhou, L.; Li, Z.; Chen, L.; Mai, L. Zn/ V_2O_5 Aqueous Hybrid-Ion Battery with High Voltage Platform and Long Cycle Life. *ACS Appl. Mater. Interfaces* **2017**, *9*, 42717–42722. [[CrossRef](#)] [[PubMed](#)]
16. Tian, Z.; Zou, Y.; Liu, G.; Wang, Y.; Yin, J.; Ming, J.; Alshareef, H.N. Electrolyte Solvation Structure Design for Sodium Ion Batteries. *Adv. Sci.* **2022**, *9*, 2201207. [[CrossRef](#)] [[PubMed](#)]
17. Liu, C.; Xie, X.; Lu, B.; Zhou, J.; Liang, S. Electrolyte Strategies toward Better Zinc-Ion Batteries. *ACS Energy Lett.* **2021**, *6*, 1015–1033. [[CrossRef](#)]
18. Wang, C.; Pei, Z.; Meng, Q.; Zhang, C.; Sui, X.; Yuan, Z.; Wang, S.; Chen, Y. Toward Flexible Zinc-Ion Hybrid Capacitors with Superhigh Energy Density and Ultralong Cycling Life: The Pivotal Role of ZnCl_2 Salt-Based Electrolytes. *Angew. Chem. Int. Ed.* **2021**, *60*, 990–997. [[CrossRef](#)]
19. Zhang, Q.; Xia, K.; Ma, Y.; Lu, Y.; Li, L.; Liang, J.; Chou, S.; Chen, J. Chaotropic Anion and Fast-Kinetics Cathode Enabling Low-Temperature Aqueous Zn Batteries. *ACS Energy Lett.* **2021**, *6*, 2704–2712. [[CrossRef](#)]
20. Cao, X.; Gao, P.; Ren, X.; Zou, L.; Engelhard, M.H.; Matthews, B.E.; Hu, J.; Niu, C.; Liu, D.; Arey, B.W.; et al. Effects of fluorinated solvents on electrolyte solvation structures and electrode/electrolyte interphases for lithium metal batteries. *Proc. Natl. Acad. Sci. USA* **2021**, *118*, e2020357118. [[CrossRef](#)]
21. Shi, J.; Xia, K.; Liu, L.; Liu, C.; Zhang, Q.; Li, L.; Zhou, X.; Liang, J.; Tao, Z. Ultrahigh coulombic efficiency and long-life aqueous Zn anodes enabled by electrolyte additive of acetonitrile. *Electrochim. Acta* **2020**, *358*, 136937. [[CrossRef](#)]
22. Nian, Q.; Wang, J.; Liu, S.; Sun, T.; Zheng, S.; Zhang, Y.; Tao, Z.; Chen, J. Aqueous Batteries Operated at -50 degrees C. *Angew. Chem. Int. Ed.* **2019**, *58*, 16994–16999. [[CrossRef](#)] [[PubMed](#)]
23. Xu, W.; Zhao, K.; Huo, W.; Wang, Y.; Yao, G.; Gu, X.; Cheng, H.; Mai, L.; Hu, C.; Wang, X. Diethyl ether as self-healing electrolyte additive enabled long-life rechargeable aqueous zinc ion batteries. *Nano Energy* **2019**, *69*, 275–281. [[CrossRef](#)]
24. Chang, N.; Li, T.; Li, R.; Wang, S.; Yin, Y.; Zhang, H.; Li, X. An aqueous hybrid electrolyte for low-temperature zinc-based energy storage devices. *Energy Environ. Sci.* **2020**, *13*, 3527. [[CrossRef](#)]
25. Huang, Z.; Wang, T.; Li, X.; Cui, H.; Liang, G.; Yang, Q.; Chen, Z.; Chen, A.; Guo, Y.; Fan, J.; et al. Small-Dipole-Molecule-Containing Electrolytes for High-Voltage Aqueous Rechargeable Batteries. *Adv. Mater.* **2022**, *34*, 2106180. [[CrossRef](#)] [[PubMed](#)]
26. Wu, S.; Su, B.; Sun, M.; Gu, S.; Lu, Z.; Zhang, K.; Yu, D.Y.W.; Huang, B.; Wang, P.; Lee, C.S.; et al. Dilute Aqueous-Aprotic Hybrid Electrolyte Enabling a Wide Electrochemical Window through Solvation Structure Engineering. *Adv. Mater.* **2021**, *33*, 2102390. [[CrossRef](#)]
27. Li, C.; Wu, W.; Shi, H.Y.; Qin, Z.; Yang, D.; Yang, X.; Song, Y.; Guo, D.; Liu, X.X.; Sun, X. The energy storage behavior of a phosphate-based cathode material in rechargeable zinc batteries. *Chem. Commun.* **2021**, *57*, 6253. [[CrossRef](#)]
28. Shi, H.Y.; Song, Y.; Qin, Z.; Li, C.; Guo, D.; Liu, X.X.; Sun, X. Inhibiting $\text{VOPO}_4 \cdot x\text{H}_2\text{O}$ Decomposition and Dissolution in Rechargeable Aqueous Zinc Batteries to Promote Voltage and Capacity Stabilities. *Angew. Chem. Int. Ed.* **2019**, *58*, 16057–16061. [[CrossRef](#)]
29. Chen, Y.; Kang, Y.; Zhao, Y.; Wang, L.; Liu, J.; Li, Y.; Liang, Z.; He, X.; Li, X.; Tavajohi, N.; et al. A review of lithium-ion battery safety concerns: The issues, strategies, and testing standards. *J. Energy Chem.* **2021**, *59*, 83–99. [[CrossRef](#)]
30. Wang, X.; Zhang, X.; Zhao, G.; Hong, H.; Tang, Z.; Xu, X.; Li, H.; Zhi, C.; Han, C. Ether-Water Hybrid Electrolyte Contributing to Excellent Mg Ion Storage in Layered Sodium Vanadate. *ACS Nano* **2022**, *16*, 6093–6102. [[CrossRef](#)]
31. Li, M.; Hicks, R.P.; Chen, Z.; Luo, C.; Guo, J.; Wang, C.; Xu, Y. Electrolytes in Organic Batteries. *Chem. Rev.* **2023**, *123*, 1712–1773. [[CrossRef](#)]
32. Jayalakshmi, M.; Rao, M.M.; Venugopal, N.; Kim, K.-B. Hydrothermal synthesis of SnO_2 - V_2O_5 mixed oxide and electrochemical screening of carbon nano-tubes (CNT), V_2O_5 , V_2O_5 -CNT, and SnO_2 - V_2O_5 -CNT electrodes for supercapacitor applications. *J. Power Sources* **2007**, *166*, 578–583. [[CrossRef](#)]
33. Wei, T.T.; Peng, Y.Q.; Mo, L.E.; Chen, S.H.; Ghadari, R.; Li, Z.Q.; Hu, L.H. Modulated bonding interaction in propanediol electrolytes toward stable aqueous zinc-ion batteries. *Sci. China Mater.* **2022**, *65*, 1156–1164. [[CrossRef](#)]
34. Sun, Y.; Zhou, J.; Ji, H.; Liu, J.; Qian, T.; Yan, C. Single-Atom Iron as Lithiophilic Site To Minimize Lithium Nucleation Overpotential for Stable Lithium Metal Full Battery. *ACS Appl. Mater. Interfaces* **2019**, *11*, 32008–32014. [[CrossRef](#)] [[PubMed](#)]
35. Zhao, Z.; Zhao, J.; Hu, Z.; Li, J.; Li, J.; Zhang, Y.; Wang, C.; Cui, G. Long-life and deeply rechargeable aqueous Zn anodes enabled by a multifunctional brightener-inspired interphase. *Energy Environ. Sci.* **2019**, *12*, 1938. [[CrossRef](#)]
36. Li, F.; Yu, L.; Hu, Q.; Guo, S.; Mei, Y.; Liu, Q.; He, Y.; Hu, X. Fabricating low-temperature-tolerant and durable Zn-ion capacitors via modulation of co-solvent molecular interaction and cation solvation. *Sci. China Mater.* **2021**, *64*, 1609–1620. [[CrossRef](#)]
37. Shang, Y.; Chen, N.; Li, Y.; Chen, S.; Lai, J.; Huang, Y.; Qu, W.; Wu, F.; Chen, R. An “Ether-In-Water” Electrolyte Boosts Stable Interfacial Chemistry for Aqueous Lithium-Ion Batteries. *Adv. Mater.* **2020**, *32*, 2004017. [[CrossRef](#)] [[PubMed](#)]

38. Tot, A.; Zhang, L.; Berg, E.J.; Svensson, P.H.; Kloo, L. Water-in-salt electrolytes made saltier by Gemini ionic liquids for highly efficient Li-ion batteries. *Sci. Rep.* **2023**, *13*, 2154. [[CrossRef](#)]
39. Hendricks, C.; Williard, N.; Mathew, S.; Pecht, M. A failure modes, mechanisms, and effects analysis (FMMEA) of lithium-ion batteries. *J. Power Sources* **2015**, *297*, 113–120. [[CrossRef](#)]
40. Meng, C.; He, W.; Kong, Z.; Liang, Z.; Zhao, H.; Lei, Y.; Wu, Y.; Hao, X. Multifunctional water-organic hybrid electrolyte for rechargeable zinc ions batteries. *Chem. Eng. J.* **2022**, *450*, 138265. [[CrossRef](#)]
41. He, H.; Tong, H.; Song, X.; Song, X.; Liu, J. Highly stable Zn metal anodes enabled by atomic layer deposited Al₂O₃ coating for aqueous zinc-ion batteries. *J. Mater. Chem. A* **2020**, *8*, 7836. [[CrossRef](#)]
42. Tatara, R.; Karayaylali, P.; Yu, Y.; Zhang, Y.; Giordano, L.; Maglia, F.; Jung, R.; Schmidt, J.P.; Lund, I.; Shao-Horn, Y. The Effect of Electrode-Electrolyte Interface on the Electrochemical Impedance Spectra for Positive Electrode in Li-Ion Battery. *J. Electrochem. Soc.* **2019**, *166*, A5090–A5098. [[CrossRef](#)]
43. Wu, Y.; Zhu, Z.; Shen, D.; Chen, L.; Song, T.; Kang, T.; Tong, Z.; Tang, Y.; Wang, H.; Lee, C.S. Electrolyte engineering enables stable Zn-Ion deposition for long-cycling life aqueous Zn-ion batteries. *Energy Storage Mater.* **2022**, *45*, 1084–1091. [[CrossRef](#)]
44. Li, Y.; Huang, Z.; Kalambate, P.K.; Zhong, Y.; Huang, Z.; Xie, M.; Shen, Y.; Huang, Y. V₂O₅ nanopaper as a cathode material with high capacity and long cycle life for rechargeable aqueous zinc-ion battery. *Nano Energy* **2019**, *60*, 752–759. [[CrossRef](#)]

Disclaimer/Publisher’s Note: The statements, opinions and data contained in all publications are solely those of the individual author(s) and contributor(s) and not of MDPI and/or the editor(s). MDPI and/or the editor(s) disclaim responsibility for any injury to people or property resulting from any ideas, methods, instructions or products referred to in the content.